Supporting Information

Different interfacial reactions of lithium metal chloride electrolytes with high voltage cathodes determine solid-state battery performance

Ivan Kochetkov[1], Tong-Tong Zuo[2], Raffael Ruess[2], Baltej Singh[1], Laidong Zhou[1], Kavish Kaup[1], Jürgen Janek[2], Linda Nazar[1]

[1]Department of Chemistry and the Waterloo Institute for Nanotechnology, University of Waterloo, 200 University Ave W, N2L 3G1 Waterloo, Ontario, Canada

[2]Institute of Physical Chemistry & Center for Materials Research, Justus Liebig University, Heinrich-Buff-Ring 17, 35392 Giessen, Germany

Table S1. The normalized kinetic constant *k'* of the NCM85||In/InLi SSB cells at 4.3 and 4.6 V vs. Li^+/Li. The *k'* values were calculated by normalizing *k* (**Fig. 3 D**) to $R_{cathode}$ at the beginning of the aging step.[1]

	k' ($h^{-0.5}$)	
	4.3 V vs. Li^+/Li	4.6 V vs. Li^+/Li
LYZC	0.14 ± 0.04	0.40 ± 0.03
LIC	0.47 ± 0.12	0.27 ± 0.03
LSIC	0.0028 ± 0.005	0.14 ± 0.01

Table S2. Enthalpy of the interfacial reaction between $Li_{1-x}NiO_2$ and Li-M-Cl (M = In, Sc) (eV/atom) calculated with respect to the formation of M_2O_3.

		Reaction Products	**Reaction Energy per atom of reactant, ΔE_{rxt} (eV/atom)**
$LiNiO_2$	Li_3InCl_6	$LiClO_4$, NiO, LiCl, In_2O_3	-0.071
	$Li_{2.125}Sc_{0.375}In_{0.25}Cl_4$	$LiClO_4$, NiO, LiCl, In_2O_3, Sc_2O_3	-0.0092
$Li_{0.75}NiO_2$	Li_3InCl_6	$LiClO_4$, NiO, LiCl, In_2O_3	-0.075
	$Li_{2.125}Sc_{0.375}In_{0.25}Cl_4$	$LiClO_4$, NiO, LiCl, In_2O_3, Sc_2O_3	-0.093
$Li_{0.5}NiO_2$	Li_3InCl_6	$LiClO_4$, NiO, LiCl, In_2O_3	-0.080
	$Li_{2.125}Sc_{0.375}In_{0.25}Cl_4$	$LiClO_4$, NiO, LiCl, In_2O_3, Sc_2O_3	-0.095
$Li_{0.25}NiO_2$	Li_3InCl_6	$LiClO_4$, NiO, LiCl, In_2O_3	-0.103
	$Li_{2.125}Sc_{0.375}In_{0.25}Cl_4$	$LiClO_4$, NiO, LiCl, In_2O_3, Sc_2O_3	-0.112

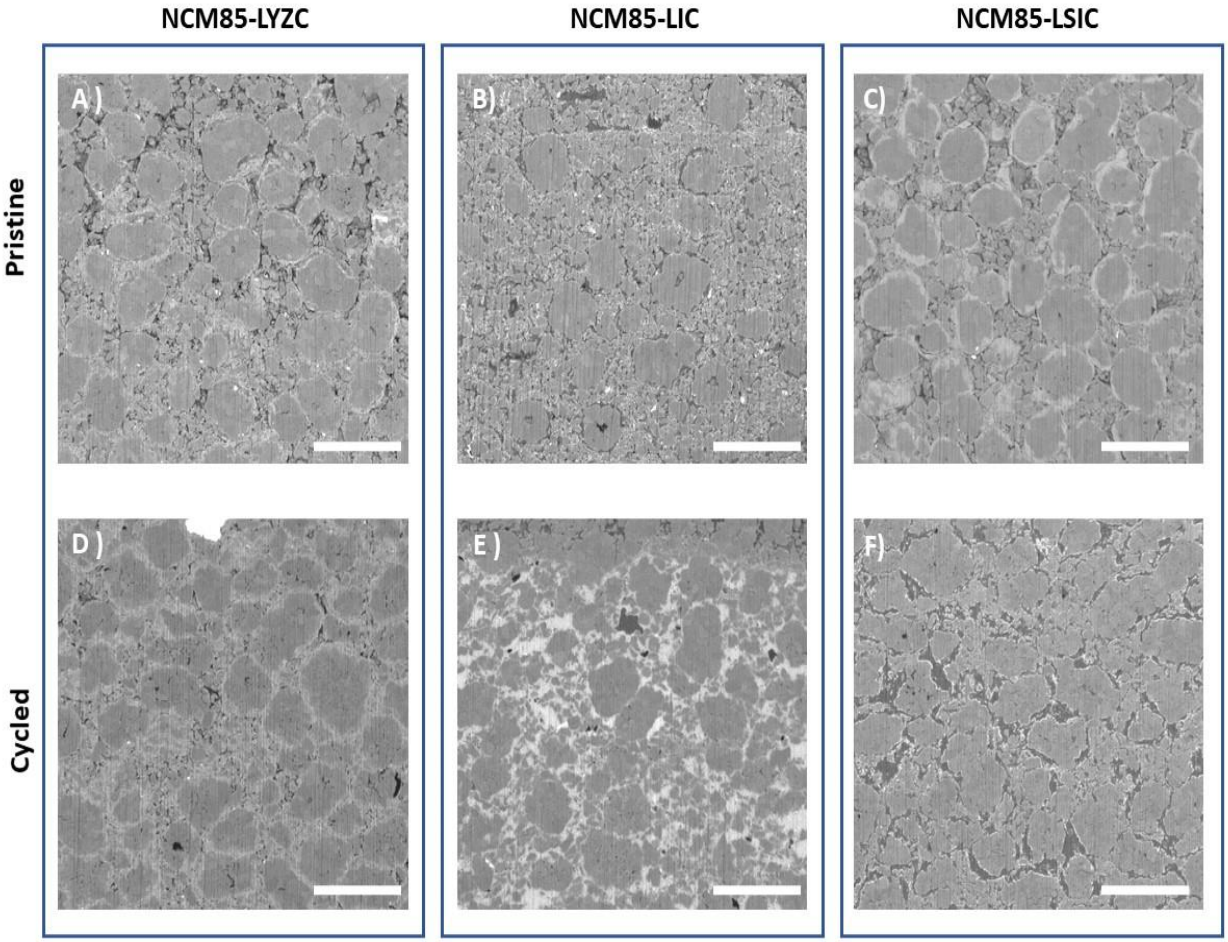

Figure S1. (A-C) Back-scattered electron images of the as-prepared NCM85 cathode composites with (A) LYZC, (B) LIC, and (C) LSIC SEs. (D-F) Back-scattered electron images of the cycled NCM85 cathode composites with (D) LYZC, (E) LIC, and (F) LSIC SEs.

The NCM85||In/InLi SSBs were cycled at room temperature (25 °C) at 0.2 C rate between 2.7 and 4.3 V vs Li^+/Li. for 120 cycles. The lesser deformation of the cycled (D) NCM85-*LYZC* composite arises from the capacity fading of the corresponding SSB upon long-term cycling. The scale bar is 5 μm.

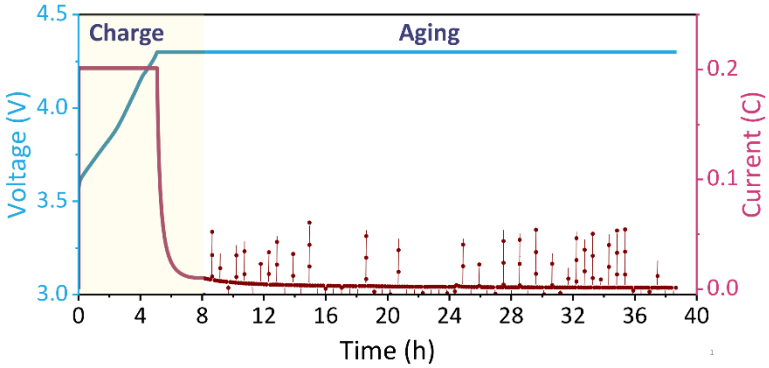

Figure S2. Aging of a NCM85||In/InLi SSB cell (representative experiment).

The NCM85||In/InLi SSB cell with LIC SE was charged to 4.3 V vs. Li^+/Li at 0.2 C and then held at the same voltage (left blue Y-axis) until the current dropped to C/100, as indicated by the right Y-axis (wine) (the shaded area from 0 to 8 hours). Then EIS was measured every hour while holding the SSB cells at 4.3 V vs. Li^+/Li.

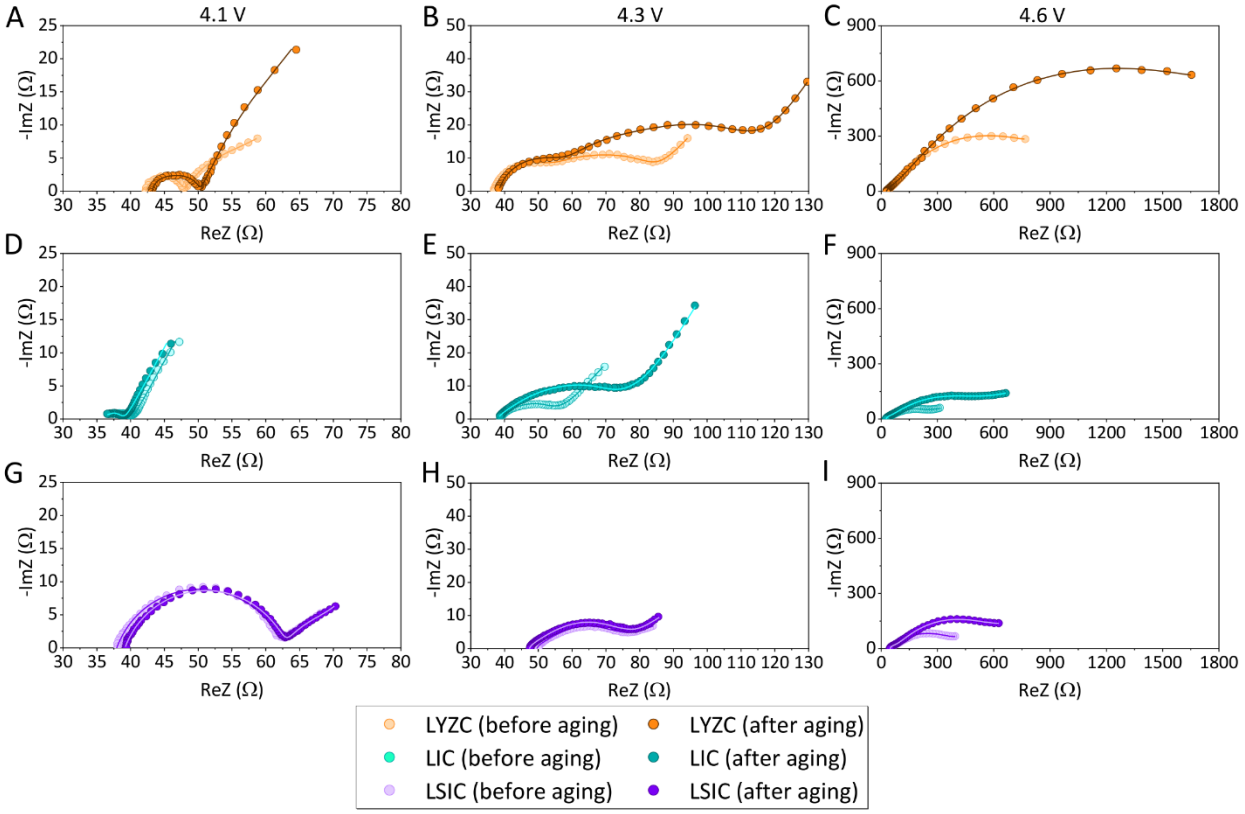

Figure S3. The effect of the composition of halide SEs and storage voltage on the stability of EIS of NCM85||In/InLi SSB cells.

(A-C) EIS of NCM85||In/InLi SSB cells with LYZC electrolyte before and after aging at (A) 4.1 V, (B) 4.3 V, and (C) 4.6 V vs. Li^+/Li.

(D-F) EIS of NCM85||In/InLi SSB cells with LIC electrolyte before and after aging at (D) 4.1 V, (E) 4.3 V, and (F) 4.6 V vs. Li^+/Li.

(G-I) EIS of NCM85||In/InLi SSB cells with LSIC electrolyte before and after aging at (G) 4.1 V, (H) 4.3 V, and (I) 4.6 V vs. Li^+/Li.

Impedance spectra recorded from 1 MHz to 0.1 mHz. The solid lines illustrate fitting with the equivalent circuit shown in **Fig. 2A.**

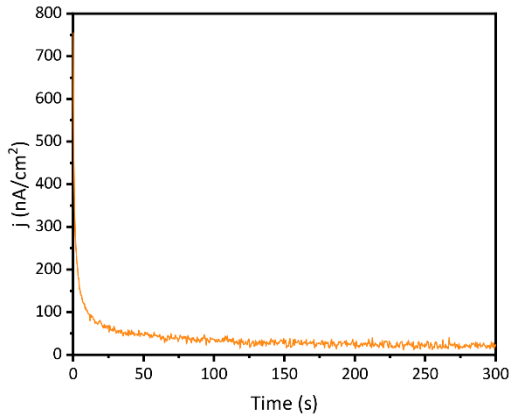

Figure S4. DC polarization experiment with a symmetric Ti|LYZC|Ti cell at 1 V and 25 °C.

LYZC powder was pressurized into a pellet with a thickness (*h)* of 420 µm at 255 MPa and then polarized at a constant voltage (*V*) of 1 V under ion-blocking conditions. The steady-state current density (j_{SS}) of (25 ± 5) nA/cm^2 was used to calculate the electronic conductivity (σ_{el}) of the SE: $\sigma_{el} = (j_{SS} \cdot h)/V$. The electronic conductivity of LYZC results as $\sigma_{el} \approx (1.1 \pm 0.3) \cdot 10^{-9}$ S/cm.

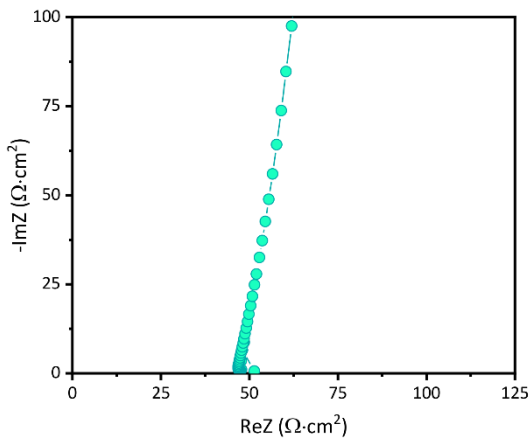

Figure S5. Nyquist plot for LIC SE at 25 °C measured in a symmetric Ti|LIC|Ti cell.

LIC powder was pressurized into a pellet with a thickness (*h)* of 790 µm at 255 MPa, and then EIS with a voltage amplitude of 100 mV was measured between 1 MHz and 1 kHz. The positive offset of the real part (~ 47 Ω·cm^2) is the bulk resistance (R_{bulk}) of the SE. The ionic conductivity (σ_{ion}), calculated as $\sigma_{ion} = h/R_{bulk}$, is σ_{ion} = 1.6 mS/cm.

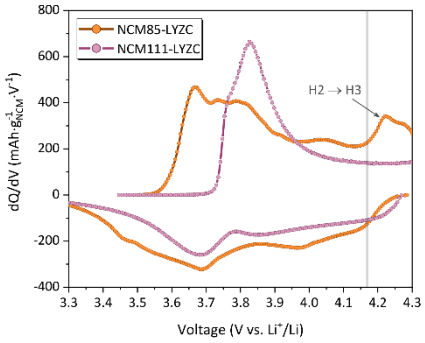

Figure S6. *dQ*/*dV* curves of the 1st cycle of NCM111||In/InLi and NCM85||In/InLi SSB cells with LYZC SE.

The SSB cells were cycled at 0.2 C between 2.7 and 4.3 V vs. Li^+/Li. The grey line (~4.17 V) points to the onset of the H2→H3 phase transition at 4.22 V, which is responsible for the capacity fading of the NCM85||In/InLi SSB cells with LYZC SE.

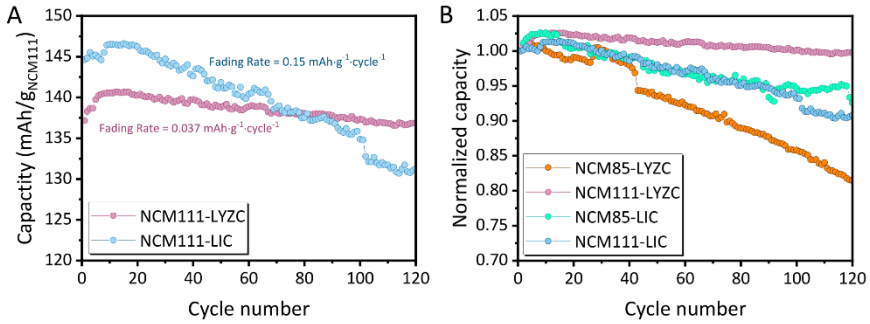

Figure S7. The capacity retention of NCM111||In/InLi and NCM85||In/InLi SSB cells cycled at 0.2 C rate between 2.7 and 4.3 V vs. Li^+/Li

(A) The absolute discharge capacity of NCM111||In/InLi cycled with LYZC and LIC SEs.

(B) The normalized capacity of the NCM111||In/InLi and NCM85||In/InLi SSBs cycled with LYZC and LIC SEs.

While the fading rate of the NCM||In/InLi with LIC SE is similar, the NCM111||In/InLi with LYZC SE exhibits much better stability than NCM85-*LYZC*.

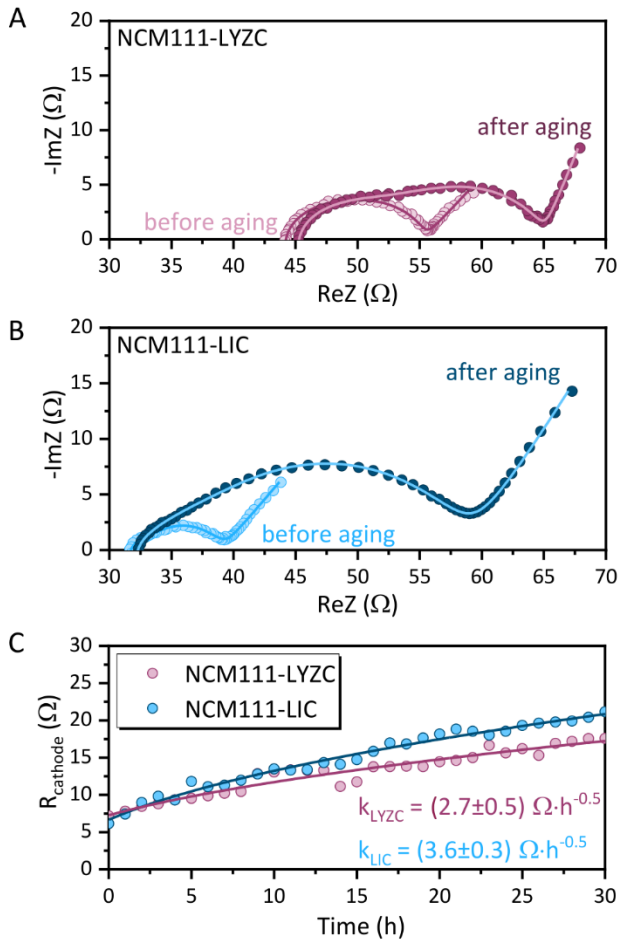

Figure S8. (A-B) Nyquist plots of the NCM111||In/InLi SSB cells with (A) LYZC and (B) LIC SEs before and after the aging at 4.3 V vs. Li^+/Li. The solid lines represent the fitting with the equivalent circuit from **Fig. 2A**. (C) Temporal evolution of $R_{cathode}$ fitted with a parabolic growth function

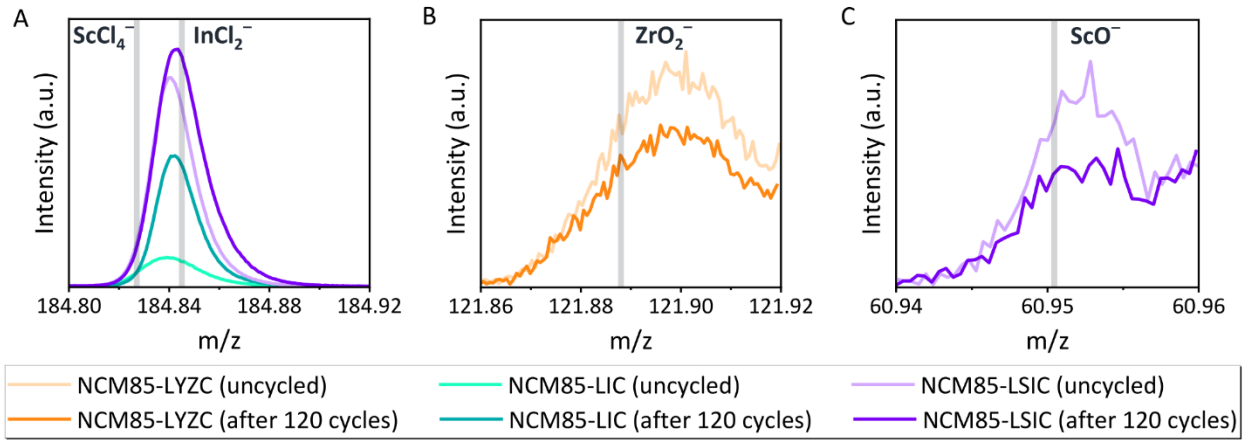

Figure S9. (A) Evolution of the fragments with the *m*/*z* ratio from 184.80 to 184.92 with cycling: $ScCl_4^-$ generated by the NCM85-LSIC cathode and $InCl_2^-$ generated by both NCM85-LIC and NCM85-LSIC cathode. (B, C) Evolution of the fragments with the *m*/*z* ratio (B) from 121.86 to 121.92 upon cycling of the NCM85||In/InLi SSB cell with LYZC electrolyte, and (C) from 60.94 to 60.96 upon cycling of the NCM85||In/InLi SSB cell with LSIC electrolyte. The SSB cells were cycled at a 0.2 C rate between 2.7 and 4.3 V vs. Li^+/Li. The grey lines at (B) 121.89 and (C) 60.95 show the expected positions of (B) ZrO_2^- and (C) ScO^-. The lack of distinguishable peaks generated by the oxides indicates that ZrO_2 and Sc_2O3 cannot be detected by ToF-SIMS.

References

(1) Zuo, T.-T.; Rueß, R.; Pan, R.; Walther, F.; Rohnke, M.; Hori, S.; Kanno, R.; Schröder, D.; Janek, J. A Mechanistic Investigation of the $Li_{10}GeP_2S_{12}$| $LiNi_{1-x-y}Co_xMn_yO_2$ Interface Stability in All-Solid-State Lithium Batteries. *Nature Comm.* **2021**, *12* (1), 1–10.